Incorporating LLM-Derived Information into Hypothesis Testing for Genomics Applications

Jordan G. Bryan, Hongqian Niu and Didong Li
Department of Biostatistics, The University of North Carolina at Chapel Hill

Abstract

We propose strategies for incorporating the information in large language models (LLMs) into statistical hypothesis tests in genomics studies. Using gene embeddings derived from text inputs to OpenAI's GPT-3.5 model, we show that biological signals in a variety of genomics datasets reside near the principal subspace spanned by the embeddings. We then use a frequentist and Bayesian (FAB) framework to propose three hypothesis tests that are optimal with respect to prior information based on the gene embedding subspace. In three separate real-world genomics examples, the FAB tests guided by the LLM-derived information achieve more power than classical counterparts.

Keywords: Frequentist and Bayesian hypothesis testing, gene embedding, type I error control.

1 Introduction

In the past decade, foundation models based on deep convolutional neural networks such as ResNet (He et al., 2016) or large transformer networks such as Google's BERT (Kenton and Toutanova, 2019) and OpenAI's GPT family (Radford, 2018) have revolutionized the analysis of data across fields such as computer vision and natural language processing. In addition to their commercial applications, these models have been shown to be valuable aids in scientific discovery in areas ranging from language understanding and translation (Vaswani et al., 2023) to multi-modal biomedical applications such as medical imaging (Li et al., 2024), drug prediction (Zhang et al., 2024), and analysis of genomic data (Cui et al., 2024; Theodoris et al., 2023; Chen and Zou, 2023).

Foundation models for genomics applications can be roughly divided into two categories: those that are trained on enormous corpora of experimental data and those that are trained on internet-scale databases of natural language, which may be filtered to include only biology-related texts (Lee et al., 2020; Gu et al., 2022) or not (Nori et al., 2023). Models that fall into the first category include the scGPT model (Cui et al., 2024), which was trained on transcriptomes from 33 million human cells from 441 different studies, curated from

the CellxGene Collection (Program et al., 2024) and the GeneFormer model (Theodoris et al., 2023), which was trained on a dataset comprised of 29.9 million human single-cell transcriptomes denoted Genecorpus-30M, collated from over 561 publicly available datasets.

While it may seem natural to construct a foundation model for biology from biological data, models that fall in the natural language category have some distinct advantages. For instance, high-quality text data are more abundant than high-quality sequencing data. Perhaps more importantly, there may be relationships between biological entities that are well-documented in the scientific literature, but which are not present in large-scale genomics datasets because they arise only in specific contexts that require bespoke experimental designs. For this reason, some recent works have used the embedding outputs of large-language models (LLMs) such as ChatGPT (Radford, 2018) to encode the biological information contained in text-based gene descriptions, such as those in the NCBI database (Schoch et al., 2020). Notably, Chen and Zou (2023) show that these text-based gene descriptors can be input to GPT-3.5 to obtain gene embeddings that act as covariates for standard prediction algorithms. For various gene-level tasks such as gene functionality class prediction, gene property prediction, and gene-gene interaction prediction, using these gene embeddings as covariates for a random forest algorithm was shown to have favorable predictive performance, even compared to that of specially pre-trained transformer models such as scGPT and GeneFormer, or BiolinkBERT (Yasunaga et al., 2022). Other works in this direction include Hou and Ji (2024), who demonstrate that GPT-4 is capable of generating cell type annotations from differential marker genes, Märtens et al. (2024) who show that incorporating prior knowledge through LLM-informed gene embeddings can achieve state-of-the-art performance on predicting unseen perturbation-induced transcriptomic changes, or Hu et al. (2024) who demonstrate the potential for pre-trained LLMs to identify gene set functions.

Based on this body of research, it is evident that LLMs are capable of producing numerical embeddings of biological entities such as genes, which capture information with relevance to a number of *prediction* tasks. Less studied to date is the potential for LLM embeddings to guide statistical *inference* in genomics contexts. In this article, we document some strategies for incorporating LLM-derived information into statistical tests of certain hypotheses that commonly arise in genomics studies. We propose three specific hypothesis tests, which have exact or approximate optimality properties with respect to the gene-to-gene similarity information encoded by LLM gene embeddings. While each of the three tests pertains to a specific parametric sampling model, all of them are motivated by the supposition that biologically meaningful signals reside on or near a subspace determined by the major axes of variation in LLM gene embeddings. Importantly, each test maintains type I error guarantees regardless of whether that supposition is accurate.

1.1 A case study in basal mRNA expression of blood cancers

We explore what it means for a biological signal to be close to a subspace determined by LLM gene embeddings through an example involving a subset of mRNA expression data downloaded from the Cancer Dependency Map (DepMap, 2024). The subset of gene expression measurements we consider consists of 728 Cancer Gene Census genes (Sondka et al., 2018) measured in 31 acute myeloid leukimia (AML) cancer cell lines and 24 B-cell acute lymphoblastic leukimia (BLL) cancer cell lines. We compute the average expression

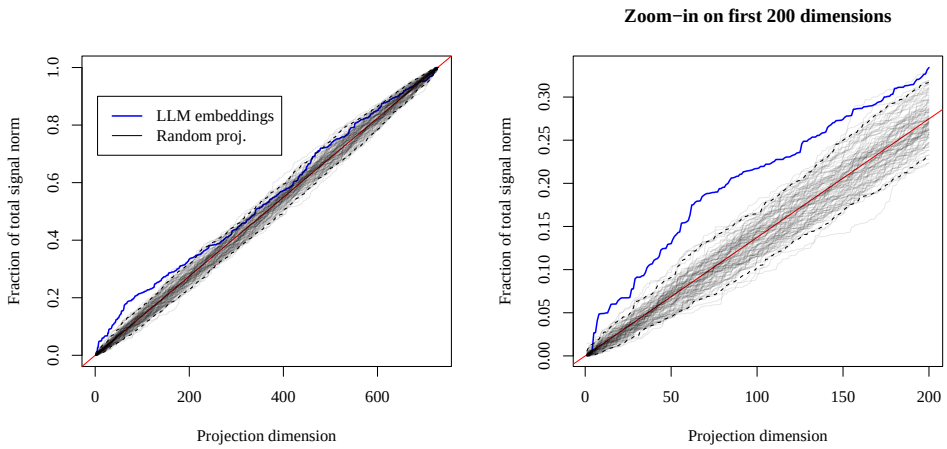

Figure 1: The quantity $\alpha_k(\mathbf{U})$ versus projection dimension k, for $k \in \{1, \ldots, 728\}$. LLM embeddings appear in blue, while random realizations of $\alpha_k(\mathbf{V})$ appear as thin, transparent lines, with dashed lines as 2.5% and 97.5% quantiles.

profiles for the AML and BLL cancer cell lines, and then take the difference between these averages to be a biological signal of interest. Along with the gene expression data, we assemble a matrix of LLM-derived gene embeddings, $\mathbf{E} \in \mathbb{R}^{728 \times 1536}$ downloaded from the GenePT repository (Chen and Zou, 2023).

Let $\mathcal{V}^{728}$ denote the set of 728×728 orthogonal matrices, let $\mathbf{U} \in \mathcal{V}^{728}$ be the orthogonal matrix of left singular vectors of $\mathbf{E}$, and let $\mathbf{y} \in \mathbb{R}^{728}$ denote the signal vector whose entries are the differences in average mRNA expression between the AML and BLL cell lines. For each $k \in \{1, \ldots, 728\}$, we evaluate the quantity

$$\alpha_k(\mathbf{U}) = \frac{\|\mathbf{U}_{1:k}^\top \mathbf{y}\|_2^2}{\|\mathbf{y}\|_2^2},$$

where $\mathbf{U}_{1:k}$ denotes the matrix consisting of the first k columns of $\mathbf{U}$. This is equal to the norm of the signal vector lying along the first k principal axes determined by the gene embeddings, relative to the total signal norm. In Figure 1, we plot $\alpha_k(\mathbf{U})$ alongside 100 realizations of the random object $\alpha_k(\mathbf{V})$ for $\mathbf{V}$ simulated from the uniform distribution on $\mathcal{V}^{728}$. In the right panel of Figure 1, we observe that the first several singular vectors of $\mathbf{E}$ capture more of the signal norm than would be expected by random projection, since the dashed lines indicate the 2.5% and 97.5% quantiles of the realizations of $\alpha_k(\mathbf{V})$.

The results of this small experiment both confirm long-standing intuition about the nature of biological signals with gene-level measurements and also indicate how LLMs might be used to detect them. Two hallmarks of modern genomic data analysis are the concepts of dimension reduction and gene-set-level analysis. Both of these approaches are motivated by the belief that in a p-dimensional measurement space where each coordinate corresponds to a gene, biologically relevant results will not appear uniformly at random within the space, but will rather tend to appear near low-dimensional subspaces that are determined by how genes relate to each other relative to the experimental context. The LLM-derived gene embeddings $\mathbf{E}$ were not designed to preferentially span any specific subspace pertaining to genes relevant to AML, BLL, or the difference between these two

cancer subtypes. Rather, it appears that the embeddings encode a general-purpose notion of gene-gene similarity, which—while not perfectly tuned for any specific experiment—may nonetheless provide some value for detecting biological signals in a variety of experimental contexts.

1.2 Article structure

In this article, we translate the general task of detecting biological signals into specific statistical hypothesis testing problems that arise in genomics studies. We then provide a means of incorporating the information in LLM-derived gene embeddings into the evaluation of each hypothesis. The methodology we propose is motivated by using the LLM information to specify a Bayesian prior distribution over the parameter indexing the null hypothesis for each test. However, the proposed hypothesis tests are assessed using the frequentist paradigm and are designed to maintain type I error control at a desired level. Hence, they are termed "frequentist and Bayesian" (FAB, Hoff, 2023).

In Section 2, we review FAB hypothesis testing and then describe three scenarios in the analysis of genomics data where FAB tests may be applied. Each scenario corresponds to a distinct hypothesis, requiring a unique FAB test statistic. Of the three tests proposed, one is a new two-sample FAB test for high dimensional means, while the others have previously appeared in the literature. In Section 3, we conduct simulation studies, focusing on the behavior of the two-sample test. In Section 4, we revisit the testing scenarios of Section 2 with applications to genomics datasets for each scenario. It is demonstrated that the FAB tests informed by LLM-derived gene embeddings achieve more power than alternative tests that do not make use of external information. We conclude with a summary of our contribution and a discussion of future work in Section 5.

2 Methods

To integrate LLM-derived information into the classical framework of statistical hypothesis testing, we use a methodology that is both frequentist and Bayesian (FAB). The three hypothesis tests we describe below are frequentist in the sense that they maintain a desired level α, while they are Bayesian in the sense that they are derived according to a criterion of maximal average power with respect to prior information. While such information may come from any source in general, here we show that the FAB approach provides a principled means to design test functions that are either optimal or approximately optimal with respect to the information derived from LLMs.

2.1 Frequentist and Bayesian (FAB) hypothesis testing

The FAB methodology was introduced by Hoff (2020). We briefly review the general principle here before describing FAB tests for specific models. Suppose we observe an m-dimensional random vector $\mathbf{y}$ having a probability distribution $P_{\boldsymbol{\theta}}$ with density $p_{\boldsymbol{\theta}}(\mathbf{y})$, both indexed by a p-dimensional parameter $\boldsymbol{\theta}$. We wish to test the hypothesis $H : \boldsymbol{\theta} = \mathbf{0}$, considering only those test functions $\phi : \mathbb{R}^m \to \{0, 1\}$ that have type I error equal to a pre-specified level α. For a simple alternative $\boldsymbol{\theta} = \boldsymbol{\theta}_1$, the Neyman-Pearson lemma (NPL)

provides the test function with maximum power:

$$\phi(\mathbf{y}) = \begin{cases} 1 & \text{if } p_{\boldsymbol{\theta}_1}(\mathbf{y})/p_{\mathbf{0}}(\mathbf{y}) > c_\alpha \\ 0 & \text{if } p_{\boldsymbol{\theta}_1}(\mathbf{y})/p_{\mathbf{0}}(\mathbf{y}) \leq c_\alpha \end{cases}, \tag{1}$$

where c_α is a constant so that $\mathrm{E}[\phi(\mathbf{y})|\boldsymbol{\theta}] = \alpha$ when $\boldsymbol{\theta} = \mathbf{0}$. An appropriate test statistic for H may then be derived from the likelihood ratio $p_{\boldsymbol{\theta}_1}(\mathbf{y})/p_{\mathbf{0}}(\mathbf{y})$.

The FAB approach derives test statistics for H according to a different kind of likelihood ratio, one which incorporates prior information about $\boldsymbol{\theta}$. For our purposes, this prior information will be a function of LLM text embeddings $\mathbf{E}$, so we represent this knowledge via a probability distribution having density $\pi_{\mathbf{E}}$. On average with respect to $\pi_{\mathbf{E}}$, a test function ϕ has power

$$\begin{aligned} \mathrm{E}[\phi(\mathbf{y})] &= \int\int \phi(\mathbf{y}) p_{\boldsymbol{\theta}}(\mathbf{y}) \pi_{\mathbf{E}}(\boldsymbol{\theta}) d\mathbf{y} d\boldsymbol{\theta} \\ &= \int \phi(\mathbf{y}) \left[\int p_{\boldsymbol{\theta}}(\mathbf{y}) \pi_{\mathbf{E}}(\boldsymbol{\theta}) d\boldsymbol{\theta} \right] d\mathbf{y} \\ &= \int \phi(\mathbf{y}) p_{\pi_{\mathbf{E}}}(\mathbf{y}) d\mathbf{y}, \end{aligned} \tag{2}$$

where $p_{\pi_{\mathbf{E}}}(\mathbf{y})$ is the marginal density of $\mathbf{y}$ under $\pi_{\mathbf{E}}$. Invoking NPL again, the level-α test that maximizes (2) rejects H when the likelihood ratio $p_{\pi_{\mathbf{E}}}(\mathbf{y})/p_{\mathbf{0}}(\mathbf{y})$ is greater than its $1-\alpha$ quantile assuming the null distribution $\mathbf{y} \sim P_{\mathbf{0}}$. Such a test is FAB because among all frequentist level-α tests for H it is the Bayes-optimal test with respect to the LLM-derived information in $\pi_{\mathbf{E}}$. As it is often more convenient to work in terms of the log-likelihood ratio $\log p_{\pi_{\mathbf{E}}}(\mathbf{y}) - \log p_{\mathbf{0}}(\mathbf{y})$ instead of the likelihood ratio itself, we do so for the tests derived in the following sections.

2.2 A FAB test for high dimensional means

In this section we develop a FAB test for the two-sample multivariate mean hypothesis testing problem that uses prior information derived from LLM text embeddings. Our primary interest lies in applications to perturbation screens in genomics, in which a high-dimensional phenotype such as mRNA expression for thousands of genes is recorded for both treated and untreated samples of cells. In the context of a high-throughput screen where treatments consist of small molecules or gene edits of unknown effect, one question of interest is whether the average gene expression profiles between the treated and untreated cell populations differ at all. Answering this question distinguishes perturbations that show evidence of bioactivity from those that appear to be inert.

To motivate the FAB test for a single perturbation, we assume the sampling model

$$\mathbf{x}_{i,j} \sim N_p(\boldsymbol{\mu}_j, \boldsymbol{\Sigma}),\ i = 1, \ldots, n_j,\ j = 1, 2,$$

where $\mathbf{x}_{i,j}$ represents the ith gene expression profile from treatment category j, and $j = 1$ corresponds to "untreated." The hypothesis we want to test is $H : \boldsymbol{\mu}_1 = \boldsymbol{\mu}_2$. For now, let $\boldsymbol{\Sigma}$ be known, so that $\mathbf{y} := \bar{\mathbf{x}}_1 - \bar{\mathbf{x}}_2$ is sufficient for $\boldsymbol{\theta} := \boldsymbol{\mu}_1 - \boldsymbol{\mu}_2$, and we may simplify the problem to testing $H : \boldsymbol{\theta} = \mathbf{0}$ with

$$\mathbf{y} \sim N_p(\boldsymbol{\theta}, \eta\boldsymbol{\Sigma}), \tag{3}$$

and $\eta = 1/n_1 + 1/n_2$. We encode the belief that biologically meaningful differences in average gene expression profiles between treated and untreated cell populations will be close to the principal subspace described by the LLM embeddings using the prior distribution

$$\boldsymbol{\theta} \sim N_p(\mathbf{0}, \nu \mathbf{E}\mathbf{E}^\top + \gamma \mathbf{I}_p). \tag{4}$$

Now, we can directly apply the reasoning from Section 2.1 (with $m = p$) to obtain an oracle FAB test for H.

Proposition 1. *The level-α FAB test of H corresponding to sampling model* (3) *and prior distribution* (4) *rejects when the test statistic*

$$T_{\text{FAB}}(\mathbf{y}) = \mathbf{y}^\top \boldsymbol{\Sigma}^{-1}[\eta(\nu \mathbf{E}\mathbf{E}^\top + \gamma \mathbf{I}_p)^{-1} + \boldsymbol{\Sigma}^{-1}]^{-1}\boldsymbol{\Sigma}^{-1}\mathbf{y}$$

exceeds its $1 - \alpha$ quantile under H.

The null distribution of $T_{\text{FAB}}(\mathbf{y})$ is that of a weighted sum of p independent χ^2_1 random variables, where the weights are equal to $1/(\eta\lambda_j + 1)$ for $j = 1, \ldots, p$, and λ_j is equal to the jth eigenvalue of $\boldsymbol{\Sigma}^{1/2}(\nu \mathbf{E}\mathbf{E}^\top + \gamma \mathbf{I}_p)^{-1}\boldsymbol{\Sigma}^{1/2}$. If $\boldsymbol{\Sigma}$ is known, then the quantiles of this distribution may be approximated with high precision using Monte Carlo.

In practical settings, $\boldsymbol{\Sigma}$ will not be known. To arrive at a computable approximation to T_{FAB}, we first consider a limiting case of (4), which occurs when $\gamma \to 0$ and $\nu \to \infty$, leading to a diffuse prior distribution with all of its mass on the embedding subspace. The FAB test statistic corresponding to this limiting prior distribution, termed $T_{\text{LFAB}}(\mathbf{y})$, is given in the following proposition.

Proposition 2. *Let $\mathbf{A} = \boldsymbol{\Sigma}^{-1}\mathbf{E}$. Then*

$$T_{\text{LFAB}}(\mathbf{y}) := \lim_{\nu \to \infty} \lim_{\gamma \to 0} T_{\text{FAB}}(\mathbf{y}) = \mathbf{y}^\top \mathbf{A}(\mathbf{A}^\top \boldsymbol{\Sigma} \mathbf{A})^{-1}\mathbf{A}^\top \mathbf{y}.$$

The expression for $T_{\text{LFAB}}(\mathbf{y})$ is written to emphasize the fact that it is a projection statistic in the sense that it is invariant to right multiplications of the form $\mathbf{A} \mapsto \mathbf{A}\mathbf{G}$ for invertible $d \times d$ matrices $\mathbf{G}$. Therefore, $T_{\text{LFAB}}(\mathbf{y})$ depends only on the column space of $\mathbf{A}$, which is determined in part by the column space of the LLM embeddings. Tests based on projection statistics have been shown to have favorable power relative to other tests for differences in high dimensional means (Lopes et al., 2011; Jacob et al., 2012), which motivates this choice of prior distribution.

Approximating $T_{\text{LFAB}}(\mathbf{y})$ yields an embedding-projected version of Hotelling's T^2 statistic, which is only roughly Bayes-optimal with respect to the limiting case of (4), but which has a tractable finite-sample null distribution. Let

$$\mathbf{S} = \frac{1}{n_1 + n_2 - 2} \sum_{j=1}^{2} \sum_{i=1}^{n_j} (\mathbf{x}_{i,j} - \bar{\mathbf{x}}_j)(\mathbf{x}_{i,j} - \bar{\mathbf{x}}_j)^\top$$

be the pooled sample covariance matrix of the gene expression profiles, and suppose further that an independent estimate $\tilde{\boldsymbol{\Sigma}}^{-1}$ of $\boldsymbol{\Sigma}^{-1}$ is available. Then our proposed approximate FAB (AFAB) statistic is

$$T_{\text{AFAB}}(\mathbf{y}) = \frac{n_1 n_2}{n_1 + n_2} \mathbf{y}^\top \tilde{\mathbf{A}}(\tilde{\mathbf{A}}^\top \mathbf{S} \tilde{\mathbf{A}})^{-1}\tilde{\mathbf{A}}^\top \mathbf{y},$$

where $\tilde{\mathbf{A}} = \tilde{\mathbf{\Sigma}}^{-1}\mathbf{E}$. By the mutual independence of $\mathbf{y}, \tilde{\mathbf{A}}$, and $\mathbf{S}$, the null distribution of $T_{\text{AFAB}}(\mathbf{y})$ can be characterized by

$$\frac{n_1 + n_2 - d - 1}{d(n_1 + n_2 - 2)} T_{\text{AFAB}}(\mathbf{y}) \sim F(d, n_1 + n_2 - d - 1).$$

Therefore, a level-α test is to reject H when $T_{\text{AFAB}}(\mathbf{y})$ exceeds $\frac{d(n_1+n_2-2)}{n_1+n_2-d-1}$ times the $1-\alpha$ quantile of the $F(d, n_1 + n_2 - d - 1)$ distribution.

2.2.1 Choice of $\tilde{\mathbf{\Sigma}}$

As long as $\tilde{\mathbf{\Sigma}}$ is independent of $\mathbf{y}$ and $\mathbf{S}$, the test based on T_{AFAB} will have level-α regardless of the particular choice of $\tilde{\mathbf{\Sigma}}$. The power of the AFAB test, though, will vary according to the column space of $\tilde{\mathbf{\Sigma}}^{-1}\mathbf{E}$. If the naive choice of $\tilde{\mathbf{\Sigma}} := \mathbf{I}_p$ is made, T_{AFAB} is equivalent to a non-randomized version of the Lopes et al. (2011) statistic, where the projection matrix is $\mathbf{E}$ rather than a matrix of entries drawn independently from $N(0, 1)$. Alternatively, one can take a split-sample approach, reserving a fraction of the $\mathbf{x}_{i,j}$'s to estimate $\tilde{\mathbf{\Sigma}}$ independently of $\mathbf{S}$. The following proposition summarizes why it may be worthwhile to find a non-naive $\tilde{\mathbf{\Sigma}}$ that approximates the true $\mathbf{\Sigma}$.

Proposition 3. *Let $B(\tilde{\mathbf{\Sigma}})$ denote the power of the AFAB test as a function of $\tilde{\mathbf{\Sigma}}$. Then for any $\boldsymbol{\delta} = \boldsymbol{\mu}_2 - \boldsymbol{\mu}_1$ in the column space of $\mathbf{E}$*

$$B(\mathbf{\Sigma}) \geq B(\mathbf{I}_p).$$

This result conforms with our previous reasoning about the maximal power property of exact FAB tests, and it suggests that using a $\tilde{\mathbf{\Sigma}}$ that closely approximates the true $\mathbf{\Sigma}$ could result in a more powerful test than naively setting $\tilde{\mathbf{\Sigma}} := \mathbf{I}_p$. However, the split-sample approach will reduce the number of observations used to compute $\mathbf{S}$, thereby reducing the power of the corresponding test. We explore the trade-off induced by the split-sample approach both in the simulation of Section 3.

2.3 A FAB F-test for linear hypotheses

In other high-throughput screening contexts, a perturbation is applied to a panel of diverse cancer cell lines, and a univariate phenotype such as post-perturbation cell viability is recorded for each cell line. For example, the data collected by Corsello et al. (2020) consist of post-treatment cell viability scores for 905 cancer cell lines for each of 1518 drugs with both oncology and non-oncology indications. In this circumstance, it is of interest to determine which drugs produce a biologically meaningful cancer-killing pattern, especially as the killing pattern relates to genomic variables such as baseline mRNA expression.

Here we describe how LLM gene embeddings can be incorporated into tests of linear hypotheses that relate cell viability to baseline mRNA expression. To do so we adopt the FAB method of McCormack and Hoff (2023), which modifies the classical F-test to incorporate prior information. A direct application of this method would share information across perturbations to specify the FAB prior, potentially biasing the FAB test results towards mechanisms of action that are over-represented in the perturbation library. Instead,

we treat perturbations independently, and we use the LLM gene embeddings to boost power near biologically salient subspaces of $\mathbb{R}^p$.

For a single perturbation, we assume that a vector of n viability scores follows the sampling model

$$\mathbf{x} \sim N_n(\mathbf{G}\boldsymbol{\theta}, \sigma^2\mathbf{I}),$$

where $\mathbf{G} \in \mathbb{R}^{n\times p}$ is a matrix of mRNA expression values for n cell lines and p genes. The hypothesis $H : \boldsymbol{\theta} = \mathbf{0}$ corresponds to a perturbation for which the pattern of viability scores shows no discernible relationship with any linear combination of gene expression profiles. Following McCormack and Hoff (2023), we consider scale-invariant tests based on the self-normalized viability profile $\mathbf{y} = \mathbf{x}/\|\mathbf{x}\|$, which has an angular Gaussian distribution on the $n-1$ unit sphere $\mathcal{S}^{n-1}$. In contrast to the previous section, this allows us to remove dependence on the unknown σ^2 from the log likelihood ratio defining the FAB test statistic because the distribution of $\mathbf{y}$ under H is the uniform distribution on $\mathcal{S}^{n-1}$. Specifying a normal prior distribution on $\boldsymbol{\theta}$ that places mass near the embedding principal subspace

$$\boldsymbol{\theta} \sim N_p(\mathbf{0}, \nu\mathbf{E}\mathbf{E}^\top + \gamma\mathbf{I}),$$

and placing a point-mass prior distribution on $\tilde{\sigma}^2$ for σ^2, the resulting FAB statistic is

$$F_{\text{FAB}}(\mathbf{y}) = -n \log \sqrt{\mathbf{y}^\top[\mathbf{G}(\nu\mathbf{E}\mathbf{E}^\top + \gamma\mathbf{I})\mathbf{G}^\top + \tilde{\sigma}^2\mathbf{I}]^{-1}\mathbf{y}}.$$

While the null distribution of $F_{\text{FAB}}(\mathbf{y})$ does not have a simple form, its quantiles may be approximated with Monte Carlo by simulating $\mathbf{x}^{(1)}, \ldots, \mathbf{x}^{(S)} \sim$ i.i.d. $N_n(\mathbf{0}, \mathbf{I})$, and then evaluating the quantiles of $\{F_{\text{FAB}}(\mathbf{x}^{(s)}/\|\mathbf{x}^{(s)}\|)\}_{s=1}^S$. A FAB test with level arbitrarily close to α may then be performed by rejecting H when $F_{\text{FAB}}(\mathbf{y})$ exceeds the $1-\alpha$ quantile of this empirical null distribution for S large.

For embedding dimension $d < n$, we can further simplify the FAB statistic by considering the limiting case $\nu \to \infty, \gamma \to 0$ as we did in the previous section. Doing so, we obtain another embedding-projected statistic, which approximates the FAB F statistic when ν is very large relative to γ and $\tilde{\sigma}^2$.

Proposition 4. *For $d < n$, the limiting FAB F-test as $\nu \to \infty, \gamma \to 0$ rejects $H : \boldsymbol{\theta} = \mathbf{0}$ when the classical F-test rejects $H : \boldsymbol{\beta} = \mathbf{0}$ under the sampling model*

$$\mathbf{x} \sim N_n(\mathbf{G}\mathbf{E}\boldsymbol{\beta}, \sigma^2\mathbf{I}_n).$$

In Section 4.2, we apply this limiting-case FAB test to a collection of linear hypotheses concerning the Corsello et al. (2020) viability scores.

2.4 FAB t-tests for multiple scalar hypotheses

In the previous two sections, we discussed FAB tests for p-dimensional hypotheses, using information in LLM embeddings to increase power in certain directions of $\mathbb{R}^p$ where we expect biologically meaningful signals to reside. Here we describe how the FAB principle may be used to test several 1-dimensional hypotheses as may arise when performing a differential expression analysis between two samples of biological specimens. In this case, the embeddings provide a means to borrow information across the independent experiments

providing the data for each hypothesis, rather than providing a subspace on which to concentrate power for a multivariate hypothesis.

Assume that a transcriptomic measurement is recorded for each of K genes in each of 2 treatment categories with n_1, n_2 replicate experiments per category. A sampling model for the measurement corresponding to the ith replicate in the jth treatment category and kth gene is

$$x_{i,j,k} \sim N(\mu_{j,k}, \sigma_k^2),\ i = 1, \ldots, n_j,\ j = 1, 2,\ k = 1, \ldots, K,$$

where it is assumed that, conditional on the population-level means $\mu_{j,k}$, the $x_{i,j,k}$ are mutually independent. Difference scores are obtained by taking the difference between the average measurement in the two treatment categories, leading to the condensed sampling model

$$\mathbf{y} \sim N_K(\boldsymbol{\theta}, \eta \mathrm{diag}(\sigma_1^2, \ldots, \sigma_K^2)),$$

where $y_k = \frac{1}{n_2}\sum_{i=1}^{n_2} x_{i,2,k} - \frac{1}{n_1}\sum_{i=1}^{n_1} x_{i,1,k}$, $\theta_k = \mu_{2,k} - \mu_{1,k}$, and $\eta = 1/n_1 + 1/n_2$. In order to identify which genes exhibit differential transcriptomic activity, it is of interest to test the hypothesis $H_k : \theta_k = 0$ for each $k \in \{1, \ldots, K\}$.

In this scenario, we consider FAB t-tests informed by LLM-derived gene embeddings based on normal prior distributions

$$\theta_k \sim N(m_k, v_k),\ k = 1, \ldots, K,$$

where m_k and v_k are chosen to reflect the prior belief that the vector of true differences $\boldsymbol{\theta}$ will be close to the principal embedding subspace. As long as m_k and v_k are independent of y_k, an approximately Bayes-optimal test for H_k may be based on the p-value

$$p_{\mathrm{FAB}}(y_k) = 1 - |G_\nu(\sqrt{\eta} y_k/\hat{\sigma}_k + 2m_k\tilde{\sigma}/v_k) - G_\nu(-\sqrt{\eta} y_k/\hat{\sigma})|,$$

where G_ν is the CDF of the t-distribution with ν degrees of freedom, $\hat{\sigma}_k^2$ is the pooled sample variance of the transcriptomic measurements for gene k, and $\tilde{\sigma}^2$ is an independent estimate of σ^2 (Hoff, 2020). LLM-informed values of m_k and v_k may then be obtained by computing the posterior expectation and variance, respectively, of θ_k with respect to the Bayesian model

$$\begin{aligned} \mathbf{y}_{-k} &\sim N_{K-1}(\boldsymbol{\theta}_{-k}, \eta \mathrm{diag}(\sigma_1^2, \ldots, \sigma_K^2)), \\ \boldsymbol{\theta} &\sim N_K(\mathbf{0}, \nu \mathbf{E}\mathbf{E}^\top + \gamma \mathbf{I}), \end{aligned}$$

where $\mathbf{y}_{-k}$ denotes the vector consisting of all but the kth difference score. This method for FAB t-testing is analogous to that in Bryan and Hoff (2022), where more details, including those regarding adaptive selection of the prior parameters ν and γ and computation of $\tilde{\sigma}^2$, may be found.

3 Evaluation of the two-sample test on simulated data

The FAB F and univariate t-tests have previously been evaluated both on simulated and real data (Bryan and Hoff, 2022; McCormack and Hoff, 2023). Here, we evaluate the two-sample AFAB test in a variety of simulation scenarios and compare its performance to that of the randomized projection (RP) test defined in Lopes et al. (2011) using d as the projection dimension. Letting $r \in (0, 1)$, we also make a comparison between the naive

AFAB test obtained by setting $\tilde{\mathbf{\Sigma}} := \mathbf{I}_p$ and a split-sample (SS) AFAB test, obtained by computing $\mathbf{y}$ and $\mathbf{S}$ using $\lfloor rn_1 \rfloor$ and $\lfloor rn_2 \rfloor$ observations, respectively, from each sample, and using a shrinkage estimate for $\tilde{\mathbf{\Sigma}}$ of the form

$$\tilde{\mathbf{\Sigma}} := \tilde{\mathbf{S}} + \frac{p}{10(n_1 - \lfloor rn_1 \rfloor + n_2 - \lfloor rn_2 \rfloor)} \mathbf{I}_p,$$

where $\tilde{\mathbf{S}}$ is the pooled covariance matrix obtained from the $n_1 - \lfloor rn_1 \rfloor + n_2 - \lfloor rn_2 \rfloor$ observations not used to compute $\mathbf{y}$ and $\mathbf{S}$. In our assessment of the SS AFAB test, we consider values of $r \in \{0.5, 0.66, 0.8\}$.

Prior to each simulation, we specify a matrix $\mathbf{E} \in \mathbb{R}^{p \times d}$ with entries drawn independently from $N(0, 1)$ and calculate the matrix of its left singular vectors $\mathbf{U}$, which represent the gene embedding subspace used in the computation of the AFAB test statistics. We perform simulations for true error covariance matrices with two different rates of spectral decay by taking the eigenvalues of $\mathbf{\Sigma}$ to be equal to an equi-spaced sequence of p numbers between 0.1 and 1 raised to the power of 20 (fast decay) or 5 (slow decay). For both rates, the total variance is normalized so that $\text{trace}(\mathbf{\Sigma}) = 50$. Within each of these scenarios, we evaluate the average power of each test across 15 random instances of $\mathbf{\Sigma}$ and $\boldsymbol{\delta} = \boldsymbol{\mu}_2 - \boldsymbol{\mu}_1$. The random covariance matrices are computed by setting the eigenvectors of $\mathbf{\Sigma}$ equal to a $p \times p$ orthogonal matrix simulated uniformly at random from $\mathcal{V}^p$. Given a noise variance $\gamma > 0$, random unit-norm signals are simulated relative to the embedding subspace according to the following generative process.

1. Simulate $\mathbf{z} \sim N_d(\mathbf{0}, \mathbf{I}_d)$.
2. Simulate $\mathbf{v} \sim N_p(\mathbf{U}\mathbf{U}^\top \mathbf{z}, \gamma \mathbf{I}_p)$
3. Set $\boldsymbol{\delta} = \mathbf{v}/\|\mathbf{v}\|$.

For each of the 15 random instances of $\mathbf{\Sigma}, \boldsymbol{\delta}$, power is calculated as the proportion of rejected tests out of 100 realizations of the two samples $\{\mathbf{x}_{i,1}\}_{i=1}^{n_1}$, $\{\mathbf{x}_{i,2}\}_{i=1}^{n_2}$. In all simulations, $n_1 = n_2 = 50$, $p = 200$, and $d = 10$.

In Figure 2, we display the results of the simulation studies for the fast and slow decay scenarios and for each of three noise variance values $\gamma \in \{1, 2/3, 1/3\}$. Overall, we observe that the AFAB tests have higher average power than the RP test. This is due to the fact that, even for the highest noise variance scenario ($\gamma = 1$) the simulated signals lie closer to the embedding subspace than would be expected if they were simulated uniformly at random from the unit sphere in $\mathbb{R}^p$. We also note that the average power of all tests considered is higher in the fast decay scenarios, which agrees with the results from Lopes et al. (2011).

In the slow decay scenarios, the naive AFAB test (denoted AFAB in Figure 2) outperforms the SS AFAB tests, regardless of the proportion of held-out samples used. This implies that whatever power was gained by using a data-driven value of $\tilde{\mathbf{\Sigma}}$ was offset by the loss in power due to having a lower sample size for the computation of $\mathbf{y}$ and $\mathbf{S}$. However, in the fast decay scenarios, this tradeoff has the opposite result. Sample-splitting appears to confer a substantial gain in average power, especially for the $\gamma = 1$ scenario, and those gains increase as the proportion of the observations used for computation of $\tilde{\mathbf{\Sigma}}$ increases. This suggests that the SS AFAB test may be advantageous in two-sample problems for which the high-dimensional covariance matrix is approximately low-rank and the true difference in means is close to the embedding subspace.

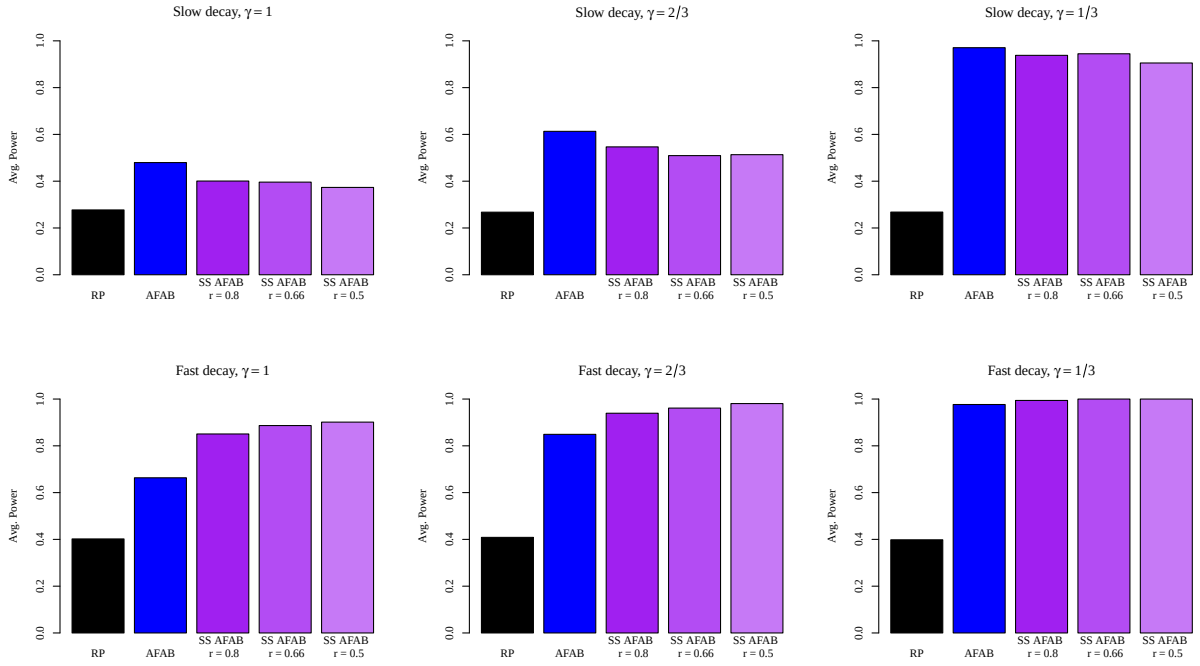

Figure 2: Results of the two-sample tests applied to simulated data in several scenarios. Spectral decay of the error covariance matrix increases from top to bottom, while average signal distance to the embedding subspace decreases from left to right.

4 Application to three tasks in cancer genomics

In real-world genomics applications, the power of the FAB tests described in Section 2 will depend on how informative the LLM-derived gene embeddings are about the space of realistic biological signals. In this section, we consider three testing scenarios in modern genomics studies and demonstrate that the corresponding FAB tests guided by the embedding subspace do provide increased power relative to classical tests that do not make use of the LLM-derived information. For each of the applications, if the number of genes considered is equal to p, the matrix $\mathbf{E}$ is a $p \times 10$ matrix of gene embeddings, obtained by taking the best rank-10 approximation of the centered and scaled $p \times 1536$ embeddings matrix downloaded from the GenePT repository.

4.1 Determination of CRISPRi bioactivity using PerturbSeq

Advances in sequencing technologies have enabled post-perturbation readouts of transcriptional activity to be achieved at genome-scale. In a landmark study, Replogle et al. (2022) used the Perturb-seq screen (Adamson et al., 2016) to record gene expression profiles for the K562 chronic myeloid leukimia (CML) cancer cell line in response to over 10000 perturbations achieved through the CRISPR interference (CRISPRi) technology. Each perturbation in this study corresponds to transcriptional suppression of a certain gene, which may or may not induce a change in the post-perturbation transcriptional state of the cell line. For downstream analyses, it is of interest to determine which perturbations show evidence of

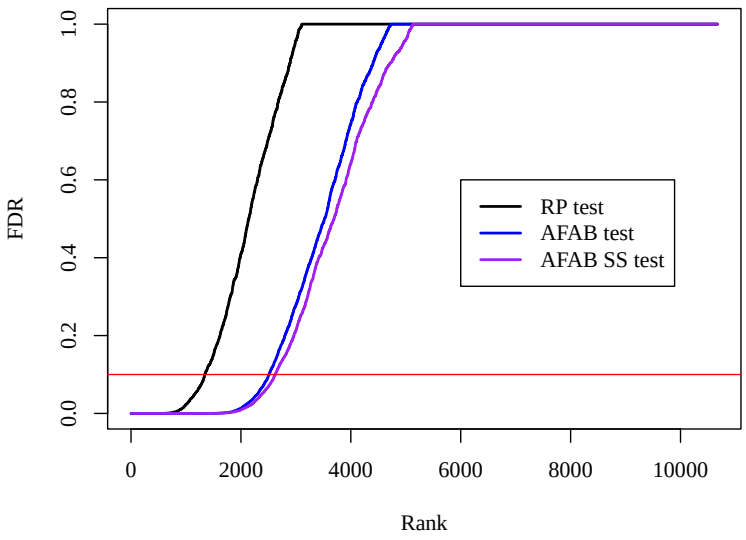

Figure 3: Sorted and adjusted p-values from the two sample tests applied to CRISPRi PerturbSeq profiles (Replogle et al., 2022). The naive AFAB test (blue) yields more discoveries than the RP test (black) at an FDR of 0.1.

inducing some transcriptional change in K562.

To address this question, we applied the two-sample AFAB test of Section 2.2 to the pseudo-bulk RNA expression profiles of Replogle et al. (2022). After filtering for genes that had GenePT embeddings available, each profile consists of $p = 7614$ measurements of mRNA expression. In total, there are 10673 unique perturbation profiles, as well as 585 profiles arising from non-targeting single-guide RNAs (sgRNAs). For the purpose of the two-sample tests, the non-targeting profiles are used as the control sample ($n_1 = 585$) and each perturbation profile is taken to be the treatment sample ($n_2 = 1$), so only the non-targeting profiles are used to compute the sample covariance $\mathbf{S}$.

In Figure 3, we plot the 10673 p-values after adjustment with the Benjamini-Hochberg procedure (Benjamini and Hochberg, 1995) obtained from each of three testing procedures: random projection (RP), naive AFAB (AFAB), and split-sample AFAB (AFAB SS) with $r = 0.66$. The random projections (RP) procedure was performed according to the steps in Lopes et al. (2011) with a projection dimension equal to 10. We observe that projection onto the embedding column space (T_{AFAB} with $\tilde{\mathbf{\Sigma}} := \mathbf{I}_p$) yields a test with more power than the RP test. The split-sample version of T_{AFAB} displays a modest further improvement in power, likely owing to the fact that the covariance matrix of the non-targeting sgRNA profiles is approximately low-rank.

4.2 Drug discovery from cell viability profiles

Pharmaceutical companies and research institutions with an interest in discovering new cancer therapies sometimes conduct high-throughput screens to determine the effect that chemical compounds in their vast libraries have on the viability of several cancer types

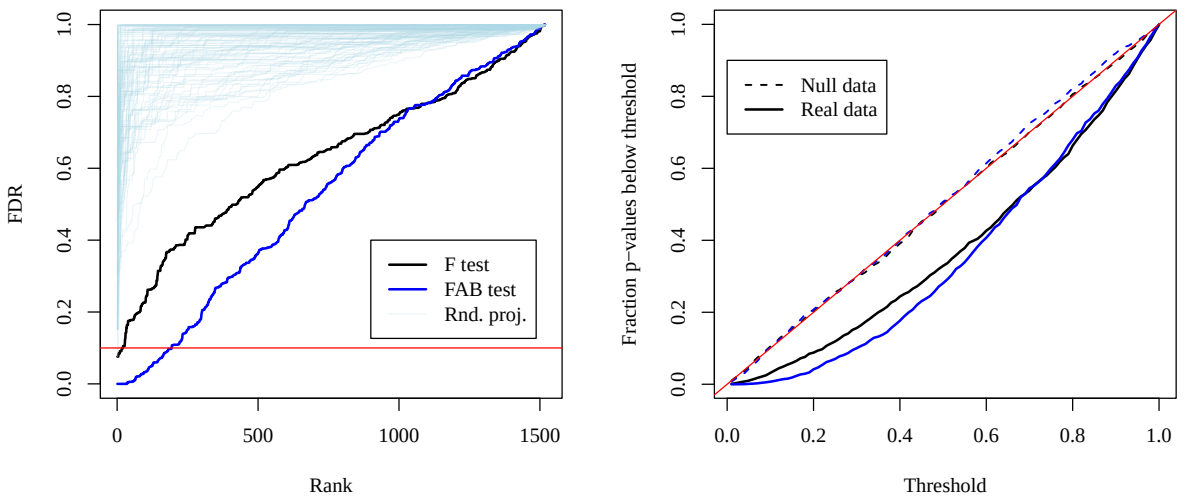

Figure 4: Sorted and adjusted p-values from F-tests applied to drug discovery data from Corsello et al. (2020). The FAB F-test (blue) yields more discoveries at an FDR of 0.1 than the classical F-test (black) and random-projection F-tests (thin, light blue).

(Broach et al., 1996; Astashkina et al., 2012). The viability effect of a drug on a particular cancer cell line is measured by the relative abundance of a stably expressed transcript in a treated sample of cells with respect to that of a control sample. While an individual viability effect may be of interest in its own right, it is often the case that a compound will be prioritized for further investigation by considering the pattern of its viability effect across multiple cell lines. This viability profile may be compared to transcriptomic data such as baseline mRNA expression in order to determine whether there is evidence of a relationship between the biological characteristics of the cancer cell lines and their response to drug treatment.

We used a cancer viability dataset from Corsello et al. (2020) to investigate whether FAB F-tests parameterized by LLM-derived gene embeddings could be useful for drug discovery in the context of a large-scale cancer viability screen. Specifically, we applied the limiting-case FAB F-test of Section 2.3 to each of 1518 drug viability profiles, using mRNA expression values from the Dependency Map as the matrix of independent variables $\mathbf{G} \in \mathbb{R}^{n \times p}$. As in Section 1.1, we considered $p = 728$ genes belonging to the Cancer Gene Census, and after filtering for common cancer cell lines between the expression dataset and the viability dataset, there were $n = 803$ cancer cell lines per viability profile.

We apply both the embedding-projected FAB F-test of Section 2.3 and the classical F-test to each of the 1518 drug viability profiles and display the results in Figure 4. In the left panel, we plot the sorted p-values obtained from the FAB and F-tests after adjustment with the Benjamini-Hochberg procedure. The classical F-test suffers from a lack of statistical power due to the large number of genes under consideration relative to the number of cancer cell lines. Only 20 drugs meet the FDR < 0.1 criterion according to the F-test, while 193 drugs do so for the FAB test. In light blue, we also plot the adjusted p-values corresponding to FAB tests performed using embedding matrices with entries simulated

independently from $N(0,1)$. This method of random projection evidently performs worse than the classical F-test, demonstrating that the increase in power of the FAB test is achieved not merely through dimension reduction, but through the particular manner of dimension reduction determined by the LLM-derived matrix of gene embeddings. In the right panel of Figure 4, the empirical CDFs of both the FAB and classical p-values show type-I error control at the nominal level for data simulated from the null distribution, while the FAB p-values are stochastically smaller than the classical p-values for the drug viability data.

4.3 Analysis of differential dependency in AML

In a final illustration of how gene embeddings derived from LLMs can guide statistical hypothesis testing in genomics studies, we consider a differential dependency analysis between 10 Ras-mutant and 8 Ras-wild-type AML cancer cell lines using data from Wang et al. (2017). In this study, CRISPR dependency scores in each AML cell line were recorded for a set of $K = 132$ gene-knockouts comprised of several known Ras interactors. As mutations in the Ras family of genes are common signatures of treatment-resistant cancer (Cox et al., 2014), it is of interest to determine which of the gene-knockouts produce a significant effect on Ras-mutant AML viability relative to that observed in the Ras-wild-type AML cell lines.

To address this question, we applied the FAB methodology of Section 2.4 to testing the hypothesis that there is no difference in average viability between Ras-mutant AML and Ras-wild-type AML upon deletion of the kth gene for each $k \in \{1, \ldots, K\}$. For comparison, we also evaluated each of these hypotheses with the classical two-sided t-test. As shown in Figure 5, the FAB t-tests rejected more null hypotheses than the classical t-tests at an FDR of 0.1 after p-value adjustment. Interestingly, one of the genes discovered only by the FAB t-tests is *KRAS*, a member of the Ras family. Gene-knockout of *KRAS* is known to be preferentially lethal to Ras-mutants (Meyers et al., 2017), so its inclusion in the list of discoveries is to be expected. The genes *GNG5* and *FURIN* also have putative relationships with Ras family members (Wu et al., 2019; He et al., 2020) and were also only discovered by the FAB t-tests.

5 Discussion

A recent review article identified exploratory embedding analysis, prediction, and transfer learning as key uses of LLM-derived information for discovery in the biological sciences (Simon et al., 2024). In this article, we demonstrated that statistical inference may be added to the list of tasks for which LLM-derived information may improve discovery in genomics studies. One of the challenges associated with performing statistical inference using information from LLMs is the "black-box" nature of that information. While the relationships between LLM-derived embeddings may be interpreted in terms of the entities they encode, the embeddings themselves have no straightforward interpretation in the absence of other data, which renders parametric models that use these embeddings as direct inputs largely uninterpretable. Our strategy for inference was to employ a FAB methodology for hypothesis testing, which uses the LLM information indirectly by focusing power for interpretable parametric hypotheses on regions of genomic space spanned by the

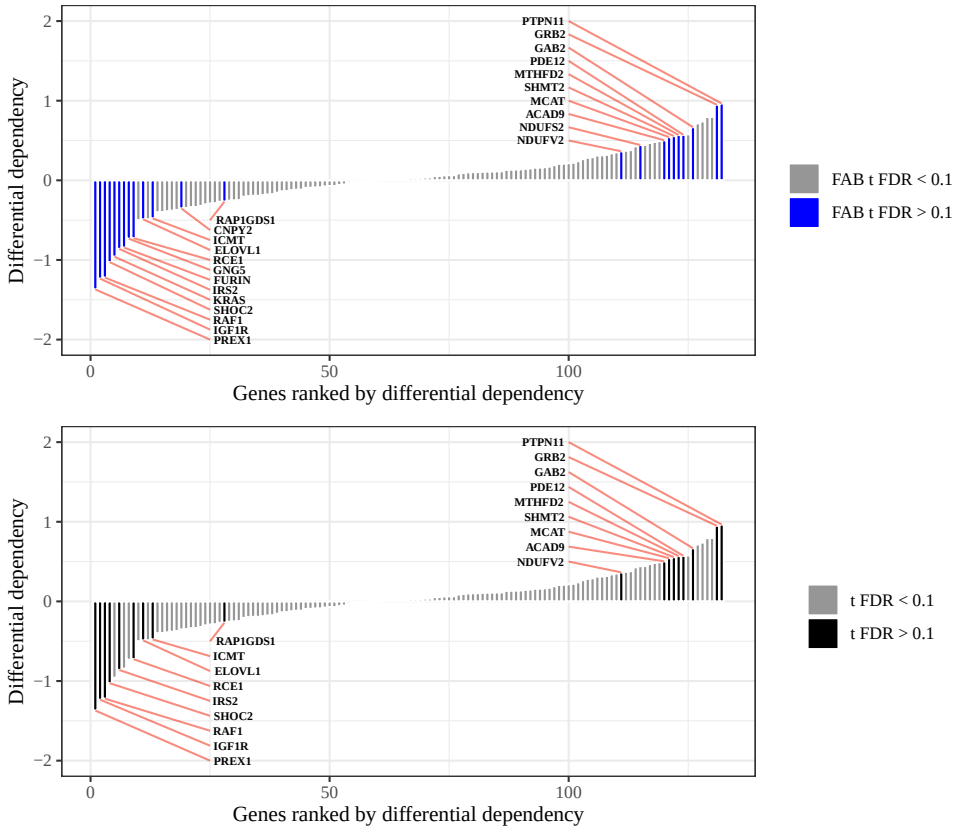

Figure 5: Results of differential dependency analysis between Ras-mutant and Ras-wild-type cancer cell lines from Wang et al. (2017). FAB t-tests (top) yield more discoveries than classical two-sided t-tests (bottom) at an FDR of 0.1.

LLM-derived gene embeddings. A key feature of the FAB hypothesis tests we proposed in this article is that they retain type I error control, regardless of the utility of the LLM-derived information.

Interestingly, the real-data examples we examined suggest that that there is indeed useful information in the LLM-derived gene embeddings as pertains to a variety of genomics contexts. The increase in power we observed in the three applications of Section 4 can be ascribed to the fact that biological signals arising in the Replogle et al. (2022), Corsello et al. (2020), and Wang et al. (2017) datasets lie close to the subspace spanned by the principal axes of the gene embeddings. The results presented in this article open several venues for further investigation.

1. **Exploring alternative LLM-derived embeddings.** While we employed gene embeddings from GenePT model in this study, these embeddings are not the only possible representation of gene information. Investigating how embeddings derived from other models, such as GPT-4 or biology-specific models like BioBERT, impact hypothesis testing performance could provide additional insights into what types of LLM information are valuable for different hypothesis testing contexts. Additionally, assessing how embeddings trained on multimodal data (e.g., integrating textual and experimental data) influence the statistical properties of FAB tests is a promising

direction.

2. **Incorporating nonlinear functions of gene embeddings.** The FAB tests proposed in this article exploit linear relationships between the GenePT embeddings and biological signals. Extending these methods to incorporate nonlinear functions of the gene embeddings as prior parameters could increase the flexibility of the FAB tests and potentially capture more complex biological relationships that are encoded in the embeddings.

3. **Developing adaptive FAB tests for high-dimensional signals.** In part for computational reasons, this article focused on projection statistics resulting from limiting cases of FAB tests. However, in general the parameters ν and γ can be chosen in a data-driven manner, as long as the data used to set the values of these parameters are independent of the data corresponding to the hypothesis being tested. Adaptive FAB tests may guard against a loss of power in biological contexts where the LLM gene embeddings are not informative.

4. **Characterizing the information content of gene embeddings.** A deeper theoretical and empirical understanding of what LLM-derived embeddings encode about genomic relationships could enhance their utility. For instance, systematically studying how specific aspects of genomic signals (e.g., gene co-expression, functional pathways) are represented in embeddings may inform the design of future statistical methods that better exploit this information.

Acknowledgement

JB was supported by an NRSA HLB Genetic Epidemiology Training Grant (T32HL129982); HN and DL were supported by NIH Grant P30ES010126.

References

Adamson, B., Norman, T. M., Jost, M., Cho, M. Y., Nuñez, J. K., Chen, Y., Villalta, J. E., Gilbert, L. A., Horlbeck, M. A., Hein, M. Y., Pak, R. A., Gray, A. N., Gross, C. A., Dixit, A., Parnas, O., Regev, A., and Weissman, J. S. (2016). A Multiplexed Single-Cell CRISPR Screening Platform Enables Systematic Dissection of the Unfolded Protein Response. *Cell*, 167(7):1867–1882.e21.

Astashkina, A., Mann, B., and Grainger, D. W. (2012). A critical evaluation of in vitro cell culture models for high-throughput drug screening and toxicity. *Pharmacology & therapeutics*, 134(1):82–106.

Benjamini, Y. and Hochberg, Y. (1995). Controlling the False Discovery Rate: A Practical and Powerful Approach to Multiple Testing. *Journal of the Royal Statistical Society: Series B (Methodological)*, 57(1):289–300.

Broach, J. R., Thorner, J., et al. (1996). High-throughput screening for drug discovery. *Nature*, 384(6604):14–16.

Bryan, J. G. and Hoff, P. D. (2022). Smaller p-values in genomics studies using distilled auxiliary information. *Biostatistics*, 24(1):193–208.

Chen, Y. and Zou, J. (2023). GenePT: A Simple But Effective Foundation Model for Genes and Cells Built From ChatGPT.

Corsello, S. M., Nagari, R. T., Spangler, R. D., Rossen, J., Kocak, M., Bryan, J. G., Humeidi, R., Peck, D., Wu, X., Tang, A. A., Wang, V. M., Bender, S. A., Lemire, E., Narayan, R., Montgomery, P., Ben-David, U., Garvie, C. W., Chen, Y., Rees, M. G., Lyons, N. J., McFarland, J. M., Wong, B. T., Wang, L., Dumont, N., O'Hearn, P. J., Stefan, E., Doench, J. G., Harrington, C. N., Greulich, H., Meyerson, M., Vazquez, F., Subramanian, A., Roth, J. A., Bittker, J. A., Boehm, J. S., Mader, C. C., Tsherniak, A., and Golub, T. R. (2020). Discovering the anticancer potential of non-oncology drugs by systematic viability profiling. *Nat Cancer*, 1(2):235–248.

Cox, A. D., Fesik, S. W., Kimmelman, A. C., Luo, J., and Der, C. J. (2014). Drugging the undruggable RAS: Mission Possible? *Nat Rev Drug Discov*, 13(11):828–851.

Cui, H., Wang, C., Maan, H., Pang, K., Luo, F., Duan, N., and Wang, B. (2024). scgpt: toward building a foundation model for single-cell multi-omics using generative ai. *Nature Methods*, pages 1–11.

David, F. N. (1938). Extension of the markoff theorem on least squares. *Stat. Res. Memoirs*, 2:105–117.

DepMap, B. (2024). DepMap 24Q2 Public. Artwork Size: 25031191226 Bytes Pages: 25031191226 Bytes.

DepMap, B. and Kocak, M. (2024). Repurposing Public 24Q2. Artwork Size: 1484816519 Bytes Pages: 1484816519 Bytes.

Gu, Y., Tinn, R., Cheng, H., Lucas, M., Usuyama, N., Liu, X., Naumann, T., Gao, J., and Poon, H. (2022). Domain-Specific Language Model Pretraining for Biomedical Natural Language Processing. *ACM Trans. Comput. Healthcare*, 3(1):1–23. arXiv:2007.15779 [cs].

He, K., Zhang, X., Ren, S., and Sun, J. (2016). Deep residual learning for image recognition. In *Proceedings of the IEEE conference on computer vision and pattern recognition*, pages 770–778.

He, Z., Thorrez, L., Siegfried, G., Meulemans, S., Evrard, S., Tejpar, S., Khatib, A.-M., and Creemers, J. W. M. (2020). The proprotein convertase furin is a pro-oncogenic driver in KRAS and BRAF driven colorectal cancer. *Oncogene*, 39(17):3571–3587.

Hoff, P. (2020). Smaller p -values via indirect information. *Journal of the American Statistical Association*, pages 1–35.

Hoff, P. (2023). Bayes-optimal prediction with frequentist coverage control. *Bernoulli*, 29(2).

Hou, W. and Ji, Z. (2024). Assessing gpt-4 for cell type annotation in single-cell rna-seq analysis. *Nature Methods*, pages 1–4.

Hu, M., Alkhairy, S., Lee, I., Pillich, R. T., Fong, D., Smith, K., Bachelder, R., Ideker, T., and Pratt, D. (2024). Evaluation of large language models for discovery of gene set function. *Nature Methods*, pages 1–10.

Jacob, L., Neuvial, P., and Dudoit, S. (2012). More power via graph-structured tests for differential expression of gene networks. *Ann. Appl. Stat.*, 6(2).

Kenton, J. D. M.-W. C. and Toutanova, L. K. (2019). Bert: Pre-training of deep bidirectional transformers for language understanding. In *Proceedings of naacL-HLT*, volume 1, page 2. Minneapolis, Minnesota.

Lee, J., Yoon, W., Kim, S., Kim, D., Kim, S., So, C. H., and Kang, J. (2020). BioBERT: a pre-trained biomedical language representation model for biomedical text mining. *Bioinformatics*, 36(4):1234–1240. arXiv:1901.08746 [cs].

Li, X., Zhao, L., Zhang, L., Wu, Z., Liu, Z., Jiang, H., Cao, C., Xu, S., Li, Y., Dai, H., et al. (2024). Artificial general intelligence for medical imaging analysis. *IEEE Reviews in Biomedical Engineering*.

Lopes, M., Jacob, L., and Wainwright, M. J. (2011). A More Powerful Two-Sample Test in High Dimensions using Random Projection. In Shawe-Taylor, J., Zemel, R., Bartlett, P., Pereira, F., and Weinberger, K. Q., editors, *Advances in Neural Information Processing Systems*, volume 24. Curran Associates, Inc.

Märtens, K., Donovan-Maiye, R., and Ferkinghoff-Borg, J. (2024). Enhancing generative perturbation models with llm-informed gene embeddings. In *ICLR 2024 Workshop on Machine Learning for Genomics Explorations*.

McCormack, A. and Hoff, P. D. (2023). Tests of linear hypotheses using indirect information. *Can J Statistics*, 51(3):852–876.

Meyers, R. M., Bryan, J. G., McFarland, J. M., Weir, B. A., Sizemore, A. E., Xu, H., Dharia, N. V., Montgomery, P. G., Cowley, G. S., Pantel, S., Goodale, A., Lee, Y., Ali, L. D., Jiang, G., Lubonja, R., Harrington, W. F., Strickland, M., Wu, T., Hawes, D. C., Zhivich, V. A., Wyatt, M. R., Kalani, Z., Chang, J. J., Okamoto, M., Stegmaier, K., Golub, T. R., Boehm, J. S., Vazquez, F., Root, D. E., Hahn, W. C., and Tsherniak, A. (2017). Computational correction of copy number effect improves specificity of CRISPR–Cas9 essentiality screens in cancer cells. *Nature Genetics*, 49(12):1779–1784.

Nori, H., Lee, Y. T., Zhang, S., Carignan, D., Edgar, R., Fusi, N., King, N., Larson, J., Li, Y., Liu, W., Luo, R., McKinney, S. M., Ness, R. O., Poon, H., Qin, T., Usuyama, N., White, C., and Horvitz, E. (2023). Can Generalist Foundation Models Outcompete Special-Purpose Tuning? Case Study in Medicine. arXiv:2311.16452 [cs].

Program, C. C. S., Abdulla, S., Aevermann, B., Assis, P., Badajoz, S., Bell, S. M., Bezzi, E., Cakir, B., Chaffer, J., Chambers, S., et al. (2024). Cz cellxgene discover: A single-cell data platform for scalable exploration, analysis and modeling of aggregated data. *Nucleic Acids Research*, page gkae1142.

Radford, A. (2018). Improving language understanding by generative pre-training.

Replogle, J. M., Saunders, R. A., Pogson, A. N., Hussmann, J. A., Lenail, A., Guna, A., Mascibroda, L., Wagner, E. J., Adelman, K., Lithwick-Yanai, G., Iremadze, N., Oberstrass, F., Lipson, D., Bonnar, J. L., Jost, M., Norman, T. M., and Weissman, J. S. (2022). Mapping information-rich genotype-phenotype landscapes with genome-scale Perturb-seq. *Cell*, 185(14):2559–2575.e28.

Schoch, C. L., Ciufo, S., Domrachev, M., Hotton, C. L., Kannan, S., Khovanskaya, R., Leipe, D., Mcveigh, R., O'Neill, K., Robbertse, B., et al. (2020). Ncbi taxonomy: a comprehensive update on curation, resources and tools. *Database*, 2020:baaa062.

Simon, E., Swanson, K., and Zou, J. (2024). Language models for biological research: a primer. *Nat Methods*, 21(8):1422–1429.

Sondka, Z., Bamford, S., Cole, C. G., Ward, S. A., Dunham, I., and Forbes, S. A. (2018). The COSMIC Cancer Gene Census: describing genetic dysfunction across all human cancers. *Nat Rev Cancer*, 18(11):696–705.

Theodoris, C. V., Xiao, L., Chopra, A., Chaffin, M. D., Al Sayed, Z. R., Hill, M. C., Mantineo, H., Brydon, E. M., Zeng, Z., Liu, X. S., et al. (2023). Transfer learning enables predictions in network biology. *Nature*, 618(7965):616–624.

Vaswani, A., Shazeer, N., Parmar, N., Uszkoreit, J., Jones, L., Gomez, A. N., Kaiser, L., and Polosukhin, I. (2023). Attention Is All You Need. arXiv:1706.03762 [cs].

Wang, T., Yu, H., Hughes, N. W., Liu, B., Kendirli, A., Klein, K., Chen, W. W., Lander, E. S., and Sabatini, D. M. (2017). Gene Essentiality Profiling Reveals Gene Networks and Synthetic Lethal Interactions with Oncogenic Ras. *Cell*, 168(5):890–903.e15.

Woodbury, M. A. (1950). *Inverting modified matrices*. Department of Statistics, Princeton University.

Wu, V., Yeerna, H., Nohata, N., Chiou, J., Harismendy, O., Raimondi, F., Inoue, A., Russell, R. B., Tamayo, P., and Gutkind, J. S. (2019). Illuminating the Onco-GPCRome: Novel G protein–coupled receptor-driven oncocrine networks and targets for cancer immunotherapy. *J. Biol. Chem.*, 294(29):11062–11086.

Yasunaga, M., Leskovec, J., and Liang, P. (2022). Linkbert: Pretraining language models with document links. *arXiv preprint arXiv:2203.15827*.

Zhang, H., Zhou, Y., Zhang, Z., Sun, H., Pan, Z., Mou, M., Zhang, W., Ye, Q., Hou, T., Li, H., et al. (2024). Large language model-based natural language encoding could be all you need for drug biomedical association prediction. *Analytical Chemistry*, 96(30):12395–12403.

A Data and Embeddings

The datasets used for the genomic experiments are the Broad Dependency Map dataset (DepMap, 2024; DepMap and Kocak, 2024), and the Perturb-seq dataset (Replogle et al., 2022) deposited at `https://plus.figshare.com/articles/dataset/_Mapping_information-rich_genotype-phenotype_landscapes_with_genome-scale_Perturb-seq_Replogle_et_al_2022_processed_Perturb-seq_datasets/20029387`. The LLM embeddings used in all experiments are from GenePT (Chen and Zou, 2023), and were derived from the text-based NCBI (Schoch et al., 2020) gene descriptions using GPT-3.5 publically available through `https://github.com/yiqunchen/GenePT` and deposited at `https://doi.org/10.5281/zenodo.10833191`.

B Proofs

B.1 Proof of Proposition 1

Proof. Given sampling model

$$\mathbf{y} \sim N_p(\boldsymbol{\theta}, \eta\boldsymbol{\Sigma})$$

and prior distribution

$$\boldsymbol{\theta} \sim N_p(\mathbf{0}, \nu\mathbf{E}\mathbf{E}^\top + \gamma\mathbf{I}_p),$$

the level-α FAB test for $H : \boldsymbol{\theta} = \mathbf{0}$ rejects when the log-likelihood ratio

$$\log p_{\pi_{\mathbf{E}}}(\mathbf{y}) - \log p_{\mathbf{0}}(\mathbf{y})$$

exceeds its $1 - \alpha$ quantile under H. Removing terms that do not depend on $\mathbf{y}$, the log-likelihood ratio is proportional to

$$(1/\eta)\mathbf{y}^\top\boldsymbol{\Sigma}^{-1}\mathbf{y} - \mathbf{y}^\top(\eta\boldsymbol{\Sigma} + \nu\mathbf{E}\mathbf{E}^\top + \gamma\mathbf{I}_p)^{-1}\mathbf{y}.$$

Now apply the Woodbury matrix inversion identity (Woodbury, 1950) to cancel the term $(1/\eta)\mathbf{y}^\top\boldsymbol{\Sigma}^{-1}\mathbf{y}$ and obtain

$$(1/\eta^2)\mathbf{y}^\top\boldsymbol{\Sigma}^{-1}[(\nu\mathbf{E}\mathbf{E}^\top + \gamma\mathbf{I}_p)^{-1} + (1/\eta)\boldsymbol{\Sigma}^{-1}]\boldsymbol{\Sigma}^{-1}\mathbf{y},$$

which is proportional to

$$T_{\text{FAB}} = \mathbf{y}^\top\boldsymbol{\Sigma}^{-1}[\eta(\nu\mathbf{E}\mathbf{E}^\top + \gamma\mathbf{I}_p)^{-1} + \boldsymbol{\Sigma}^{-1}]\boldsymbol{\Sigma}^{-1}\mathbf{y}.$$

□

B.2 Proof of Proposition 2

Proof. From above, the relevant portion of the log-likelihood ratio is

$$(1/\eta)\mathbf{y}^\top\boldsymbol{\Sigma}^{-1}\mathbf{y} - \mathbf{y}^\top(\eta\boldsymbol{\Sigma} + \nu\mathbf{E}\mathbf{E}^\top + \gamma\mathbf{I}_p)^{-1}\mathbf{y}.$$

Set $\boldsymbol{\Psi} := \eta\boldsymbol{\Sigma} + \gamma\mathbf{I}_p$, and apply the Woodbury matrix identity to a different grouping of terms than above to obtain

$$\mathbf{y}^\top[(1/\eta)\boldsymbol{\Sigma}^{-1} - \boldsymbol{\Psi}^{-1} + \boldsymbol{\Psi}^{-1}\mathbf{E}(\mathbf{E}^\top\boldsymbol{\Psi}^{-1}\mathbf{E} + (1/\nu)\mathbf{I}_d)^{-1}\mathbf{E}^\top\boldsymbol{\Psi}^{-1}]\mathbf{y}.$$

Now, $\lim_{\gamma\to 0} \mathbf{\Psi}^{-1} = (1/\eta)\mathbf{\Sigma}^{-1}$, so the limit as $\gamma \to 0$ of the expression above is

$$(1/\eta^2)\mathbf{y}^\top[\mathbf{\Sigma}^{-1}\mathbf{E}((1/\eta)\mathbf{E}^\top\mathbf{\Sigma}^{-1}\mathbf{E} + (1/\nu)\mathbf{I}_d)^{-1}\mathbf{E}^\top\mathbf{\Sigma}^{-1}]\mathbf{y}.$$

Taking the limit of this expression as $\nu \to \infty$ yields

$$(1/\eta)\mathbf{y}^\top\mathbf{\Sigma}^{-1}\mathbf{E}(\mathbf{E}^\top\mathbf{\Sigma}^{-1}\mathbf{E})^{-1}\mathbf{E}^\top\mathbf{\Sigma}^{-1}\mathbf{y}.$$

Making the substitution $\mathbf{A} = \mathbf{\Sigma}^{-1}\mathbf{E}$ and comparing the above to T_{FAB} completes the proof. □

B.3 Proof of Proposition 3

Proof. As a function of $\tilde{\mathbf{\Sigma}}$, the power of the AFAB test is determined by the non-central $F(d, n_1 + n_2 - d - 1)$ distribution, and increases monotonically with the non-centrality parameter

$$c(\tilde{\mathbf{\Sigma}}) = \boldsymbol{\delta}^\top\tilde{\mathbf{\Sigma}}^{-1}\mathbf{E}(\mathbf{E}^\top\tilde{\mathbf{\Sigma}}^{-1}\mathbf{\Sigma}\tilde{\mathbf{\Sigma}}^{-1}\mathbf{E})^{-1}\mathbf{E}^\top\tilde{\mathbf{\Sigma}}^{-1}\boldsymbol{\delta},$$

where $\boldsymbol{\delta} = \boldsymbol{\mu}_2 - \boldsymbol{\mu}_1$. To show that the power of an oracle version of the AFAB test has greater power than the AFAB test based on $\tilde{\mathbf{\Sigma}} := \mathbf{I}_p$ for any $\boldsymbol{\delta}$ in the column space of $\mathbf{E}$, we will show that $c(\mathbf{\Sigma}) \geq c(\mathbf{I_p})$ for any such $\boldsymbol{\delta}$.

An oracle version of the AFAB test would have non-centrality parameter

$$c(\mathbf{\Sigma}) = \boldsymbol{\delta}^\top\mathbf{\Sigma}^{-1}\mathbf{E}(\mathbf{E}^\top\mathbf{\Sigma}^{-1}\mathbf{E})^{-1}\mathbf{E}^\top\mathbf{\Sigma}^{-1}\boldsymbol{\delta}.$$

Because of the invariance of the AFAB statistic, without loss of generality we can assume $\mathbf{E}$ is orthogonal. For any $\boldsymbol{\delta}$ in the column space of $\mathbf{E}$, we may write $\boldsymbol{\delta} = \mathbf{Ed}$ for some $\mathbf{d} \in \mathbb{R}^d$. Thus, the non-centrality parameter of the oracle AFAB test is

$$\begin{aligned}\boldsymbol{\delta}^\top\mathbf{\Sigma}^{-1}\mathbf{E}(\mathbf{E}^\top\mathbf{\Sigma}^{-1}\mathbf{E})^{-1}\mathbf{E}^\top\mathbf{\Sigma}^{-1}\boldsymbol{\delta} &= \mathbf{d}^\top\mathbf{E}^\top\mathbf{\Sigma}^{-1}\mathbf{E}(\mathbf{E}^\top\mathbf{\Sigma}^{-1}\mathbf{E})^{-1}\mathbf{E}^\top\mathbf{\Sigma}^{-1}\mathbf{Ed} \\ &= \mathbf{d}^\top\mathbf{E}^\top\mathbf{\Sigma}^{-1}\mathbf{Ed}.\end{aligned}$$

Compare this to the power of the AFAB test setting $\tilde{\mathbf{\Sigma}} := \mathbf{I}_p$, which is

$$\mathbf{d}^\top\mathbf{E}^\top\mathbf{E}(\mathbf{E}^\top\mathbf{\Sigma}\mathbf{E})^{-1}\mathbf{E}^\top\mathbf{Ed} = \mathbf{d}^\top(\mathbf{E}^\top\mathbf{\Sigma}\mathbf{E})^{-1}\mathbf{d}.$$

By the Gauss-Markov Theorem (David, 1938), we have

$$(\mathbf{E}^\top\mathbf{\Sigma}^{-1}\mathbf{E})^{-1} \preceq \mathbf{E}^\top\mathbf{\Sigma}\mathbf{E},$$

where $\preceq$ denotes the Loewner partial order. Therefore,

$$(\mathbf{E}^\top\mathbf{\Sigma}\mathbf{E})^{-1} \preceq \mathbf{E}^\top\mathbf{\Sigma}^{-1}\mathbf{E},$$

which shows that $c(\mathbf{\Sigma}) \geq c(\mathbf{I}_p)$. □

B.4 Proof of Proposition 4

Proof. Let $d < n$. The FAB F-test is based on the test statistic

$$F_{\text{FAB}}(\mathbf{y}) = -n \log \sqrt{\mathbf{y}^\top [\mathbf{G}(\nu \mathbf{E}\mathbf{E}^\top + \gamma \mathbf{I})\mathbf{G}^\top + \tilde{\sigma}^2 \mathbf{I}]^{-1} \mathbf{y}}.$$

When $\gamma \to 0$, we have

$$\lim_{\gamma \to 0} \; F_{\text{FAB}}(\mathbf{y}) = -n \log \sqrt{\mathbf{y}^\top [\nu \mathbf{G}\mathbf{E}\mathbf{E}^\top \mathbf{G}^\top + \tilde{\sigma}^2 \mathbf{I}]^{-1} \mathbf{y}}.$$

Let $\mathbf{Q}$, $\mathbf{\Lambda}$ be, respectively, the left singular vectors and singular values of the matrix $\mathbf{GE}$. Then

$$[\nu \mathbf{G}\mathbf{E}\mathbf{E}^\top \mathbf{G}^\top + \tilde{\sigma}^2 \mathbf{I}]^{-1} = [\mathbf{Q} \; \mathbf{Q}^\perp] \mathbf{D}^{-1} [\mathbf{Q} \; \mathbf{Q}^\perp]^\top,$$

where $\mathbf{Q}^\perp$ is an orthogonal basis for the column space of $\mathbf{I}_n - \mathbf{Q}\mathbf{Q}^\top$, and $\mathbf{D}$ is a diagonal matrix with entries $D_{ii} = \nu \lambda_i^2 + \tilde{\sigma}^2$ for $i = 1, \ldots, d$ and $D_{ii} = \tilde{\sigma}^2$ for $i = d+1, \ldots, n$. Taking $\nu \to \infty$, we have

$$(1/\tilde{\sigma}^2)(\mathbf{I}_n - \mathbf{Q}\mathbf{Q}^\top),$$

so

$$\lim_{\nu \to \infty} \lim_{\gamma \to 0} \; F_{\text{FAB}}(\mathbf{y}) = -n \log \sqrt{(1/\tilde{\sigma}^2) \mathbf{y}^\top (\mathbf{I}_n - \mathbf{Q}\mathbf{Q}^\top) \mathbf{y}}.$$

Now, both this limiting statistic and the F-statistic based on the sampling model

$$\mathbf{x} \sim N_n(\mathbf{GE}\boldsymbol{\beta}, \sigma^2 \mathbf{I}_n)$$

are strictly increasing functions of the quantity $\mathbf{y}^\top \mathbf{Q}\mathbf{Q}^\top \mathbf{y}$. Therefore, a level-$\alpha$ test based on $\lim_{\nu \to \infty} \lim_{\gamma \to 0} \; F_{\text{FAB}}(\mathbf{y})$ rejects when the level-α F-test for $H : \boldsymbol{\beta} = \mathbf{0}$ under the sampling model above rejects. $\square$